Glass Europe Vol. 1 (2023)
https://doi.org/10.52825/glass-europe.v1i.425

Submitted: 30 April 2023 | Accepted: 07 June 2023 | Published: 26 June 2023

Hydrogen Permeability of Tectosilicate Glasses for Tank Barrier Liners

S. Reinsch[1][https://orcid.org/0000-0003-3216-4635], T. Welter[2], R. Müller[1][https://orcid.org/0000-0002-1044-2035], and J. Deubener[2][https://orcid.org/0000-0002-3474-7490]

[1] Bundesanstalt für Materialforschung und -prüfung (BAM), 12489 Berlin, Germany

[2] Clausthal University of Technology, Institute of Non-Metallic Materials, 38678 Clausthal-Zellerfeld, Germany

Abstract. The permeation of hydrogen gas was studied in meta-aluminous (tectosilicate) glass powders of $Li_2O{\cdot}Al_2O_3{\cdot}SiO_2$ (LAS), $Na_2O{\cdot}Al_2O_3{\cdot}SiO_2$ (NAS) and $MgO{\cdot}Al_2O_3{\cdot}SiO_2$ (MAS) systems by pressure loading and vacuum extraction in the temperatures range 210–310 °C. With this method, both the solubility *S* and the diffusivity *D* were determined, while the permeability was given by the product *SD*. For all glasses, *S* was found to decrease with temperature, while *D* increased. Since the activation energy of diffusion of H_2 molecules exceeded that of dissolution, permeation increased slightly with temperature. When extrapolated to standard conditions (25 °C), the permeability of tectosilicate glasses was found to be only 10^{-22}–10^{-24} mol H_2 (m s Pa)$^{-1}$, which is 8–10 magnitudes lower than most polymers. Thin glass liners of these compositions are expected to be the most effective barrier for tanks of pressurised hydrogen.

Keywords: Hydrogen permeation, Aluminosilicate glasses, Hydrogen storage tank, Glass liner

1. Introduction

Glasses with meta-aluminous (tectosilicate) composition such as eucryptite ($Li_2O{\cdot}Al_2O_3{\cdot}2SiO_2$), spodumene ($Li_2O{\cdot}Al_2O_3{\cdot}4SiO_2$) and cordierite ($2MgO{\cdot}2Al_2O_3{\cdot}5SiO_2$) are the basis for commercially available glass-ceramics. Their structure consists of modifiers that fill completely polymerised silicate networks by introducing charge-balanced aluminium tetrahedra. Meta-aluminous melts are very good glass formers as they generally retain their complex polymerised structure even at high temperatures [1] and can therefore be produced by conventional melt quenching and shaped to thin (submillimetre) glasses of various geometries such as sheets and tubes by drawing.

When storing compressed hydrogen, materials with low H_2 permeability are required to minimise leakage over long standby and operating times. Hydrogen storing technologies on a volumetric basis for on-board applications, such as vehicle tanks, are currently fibre-reinforced composites with metal (type III) and polymer liners (type IV) to meet safety aspects at pressures up to 70 MPa [2], [3].

The loss of hydrogen gas through the wall of these tanks can be significantly reduced if glasses or glass liners are developed that have several orders of magnitude lower H_2 permeability than polymer matrix materials today [4]. Barth et al. [5] showed that the permeability of various polymer materials at room temperature is in the range of 10^{-14}–10^{-16} mol H_2 (m s Pa)$^{-1}$. It is known that inorganic oxide glasses are far below that limit, e.g. the archetypal silica glass has a lower permeability of 10^{-19}–10^{-20} mol H_2 (m s Pa)$^{-1}$ [6]. However, from a glass-manufacturing point of view, fused silica requires the highest temperatures (about 2000 °C), which is costly and therefore less attractive for a potential H_2 barrier liner in tanks.

Previous work has shown [7] that minimising the accessible volume is a successful strategy to further hinder the migration and solubility of H_2 molecules in the network structure of silicate glasses. Two competing approaches have been identified that achieve a reduction in the total free volume firstly by modifying the network through the creation of non-bridging oxygen (NBO) and secondly by filling or stuffing polymerised (NBO-free) silicate networks through the introduction of charge-balanced network formers such as aluminium and boron tetrahedra. While in the former (modified glass structures) the reduction in free volume and thus the decrease in permeability seems to depend on the type of modifier cation (cations with high field strength such as Li are more effective than those with low field strength), in the latter (NBO-free glasses) a tendency in favour of aluminosilicates over borosilicates can be seen [7]. Note that NBO defines an oxygen that is part of a tetrahedron but is not shared with a second tetrahedron. NBO forms the ionic bonds with the modifiers.

By changing the network structure due to the introduction of modifier cations that compensate for the charges of either NBO or tetrahedrally coordinated Al^{3+} and B^{3+}, the melting and forming temperatures drop compared to silica glass, while thermal expansion coefficients increase. Both will favour the potential application as hydrogen barrier in multi-material composites. However, highly modified network glasses, such as alkali di- and metasilicates, have limited technological suitability due to their high kinetic fragility and strong tendency to crystallise or corrode. Therefore, fully polymerised aluminosilicate glasses were investigated here. In particular, eucryptite, spodumene and cordierite glasses are studied, since these compositions have a relatively high degree of substitution of silicon by aluminium (in eucryptite glass, nominally every second silicon tetrahedron is replaced by an aluminium tetrahedron) and therefore the lowest hydrogen gas permeation can be expected. To extend the spectrum of aluminosilicate glasses with tectosilicate composition, data from earlier measurements [8] for albite ($Na_2O{\cdot}Al_2O_3{\cdot}6SiO_2$), jadeite ($Na_2O{\cdot}Al_2O_3{\cdot}4SiO_2$) and nepheline ($Na_2O{\cdot}Al_2O_3{\cdot}2SiO_2$) glasses are added. To illustrate the outstanding barrier effect of a thin layer of these tectosilicate glasses (glass liner), the effective permeation through a pressurised hydrogen tank with glass lining is calculated.

2. Experimental

2.1 Glass preparation

Three glasses of target composition $Li_2O{\cdot}Al_2O_3{\cdot}2SiO_2$ (eucryptite), $Li_2O{\cdot}Al_2O_3{\cdot}4SiO_2$ (spodumene) and $2MgO{\cdot}2Al_2O_3{\cdot}5SiO_2$ (cordierite) were melted from $Al(OH)_3$, $MgCO_3$, Li_2CO_3 and SiO_2 industrial grade raw materials (~500 g batch) in an electric furnace and stirred using PtRh20 crucibles at Schott AG, Mainz, Germany. To avoid unwanted crystallisation during pouring, the eucryptite and spodumene melts were roller quenched to receive $\leq$ 1 mm thick glass ribbons. The cordierite melt was less prone to crystallisation and was therefore poured onto a steel plate to form a ~15 mm thick glass block and cooled to the estimated glass transition temperature with 30 K h^{-1}. The chemical composition of the glasses was not analysed. However, glasses of a similar composition (+ nucleating agents), previously melted from the same raw materials and following the same time-temperature protocol, showed only minor deviations from the target composition (see Tab. 1 of Ref. [9]). For the permeation experiments, parts of the glass blocks and ribbons were crushed (steel mortar) with one or two strokes and then sieved. This process was repeated with new starting pieces until about 1.9 g of the fraction 100–125 µm was obtained, while unground parts of the ribbons and glass block were used for buoyancy measurements. The surface area of the sieved powder fraction was not studied, as preliminary tests showed that the influence of the grain shape and size distribution within the sieved 100–125 µm fraction on diffusivity and solubility experiments is negligible. In addition, eight sodium aluminosilicate glasses of a previous study were used [8]. The composition of these glasses (reports on the analyses in [8]) ranged from ~50–90 mol% SiO_2 (all with Na_2O/Al_2O_3 = 1), including compositions close to the stoichiometric tectosilicates

$Na_2O{\cdot}Al_2O_3{\cdot}2SiO_2$ (nepheline), $Na_2O{\cdot}Al_2O_3{\cdot}4SiO_2$ (jadeite) and $Na_2O{\cdot}Al_2O_3{\cdot}6SiO_2$ (albite). Furthermore, a silica glass from the same study was also examined as a reference material. Glasses were named after the element and molar percentage of the modifier cation that balances the charge of the tetrahedrally coordinated Al^{3+}. In the lithium aluminosilicate system (LAS), glasses of the eucryptite and spodumene compositions were named Li25 and Li16.7, respectively, and the cordierite glass of the magnesium aluminosilicate system (MAS) was named Mg22.2. The glasses of the sodium aluminosilicate system (NAS) were: Na5, Na10.5, Na12.1, Na14, Na16.1, Na20, Na22 and Na23.8. The density of the prepared glasses was determined according to the buoyancy method at room temperature. The weight of individual pieces (0.2–0.5 g mass) was measured in air and in ethanol. The error of this method (based on repetitive measurements) was ≤ 0.2% and resulted in the values 2.363 g cm^{-3} (Li25), 2.374 g cm^{-3} (Li16.7) and 2.620 g cm^{-3} (Mg22.2). Density of the eight sodium aluminosilicate glasses and the silica reference glass was determined previously and reported in [8].

2.2 Hydrogen gas permeation through glass

The permeability of hydrogen gas *P* was calculated from hydrogen diffusivity *D* and hydrogen solubility *S* according to [10]:

$$P = DS \tag{1}$$

D and *S* were measured with the vacuum extraction device equipped with mass spectrometry (VHE) as described in detail in [8], [11]. For this purpose, glass powders (80–105 mg) were exposed to pressurised hydrogen at different temperatures for different exposure times to ensure that the hydrogen loading was fully saturated. *D* was then determined by fitting the VHE hydrogen degassing rate dQ/dt with the classical diffusion model for isothermal degassing from a sphere [12]:

$$\frac{d}{dt}\frac{Q(t)}{Q_\infty} = \frac{6D}{r^2}\sum_{n=1}^{\infty} exp\left(-n^2\pi^2\frac{Dt}{r^2}\right) \tag{2}$$

with *t* = isothermal degassing time, *r* = radius of the glass sphere, $Q(t)$ = amount of hydrogen released at *t* and Q_0 = total amount of dissolved hydrogen. Herein, a uniform radius of glass spheres was assumed, which was taken from d_{50} of the measured particle size distribution [11]. As the ratio $Q(t)/Q_\infty$ is dimensionless, *D* was fitted in terms of I_{H2}, the VHE hydrogen ion current (in A) (Fig. 1). *S* was obtained from the same VHE degassing run as the total hydrogen amount dissolved per unit volume per unit external (loading) pressure according to [13]:

$$S = \frac{p_0}{p_L}Q_\infty = \frac{p_0}{p_L}\int_0^t \frac{dQ}{dt'}dt' = \frac{p_0}{p_L}\int_0^t C I_{H_2} dt' \tag{3}$$

with p_0 = standard pressure (≈ 1 bar), p_L = loading pressure, *C* = the VHE calibration constant (mol H_2 A^{-1} s^{-1}) and *t* = total degassing time (s) including the ramp from room temperature to the isothermal section, the waiting time at this temperature and the final ramp to 825 °C (to release the remaining, previously non-degassed hydrogen) (Fig. 1).

For the glasses Li25, Li16.7, and Mg22.2, powders of the sieve fraction 100–125 µm were exposed to hydrogen at 6 MPa and 210 °C, 260 °C and 310 °C. 24 h exposure was thoroughly applied to ensure complete saturation of the loading. The experiments were repeated up to 2 times. Since the diffusivity of the eight sodium aluminosilicate glasses and the silica reference glass had been determined previously [8], only solubility experiments were performed with powders of the sieve fraction 180–200 µm at 268 °C and the same H_2 loading pressure of 6 MPa for 16–52 h. The latter experiments were repeated up to seven times. The uncertainties of *D* and *S* determined according to the experimental powder method were factors of up to 3 and 0.7, respectively. Preliminary measurements showed that at exposure temperatures below

200 °C the amount of detectable hydrogen was too low, i.e. the lower detection limit of our instrument was reached, so that measurements at temperatures < 200 °C were not carried out.

The temperature dependence of the solubility *S*, diffusivity *D* and permeability *P* of hydrogen gas is best described by Arrhenius-type equations [14]:

$$S = S_0 exp\left(-\frac{E_S}{RT}\right), \tag{4}$$

$$D = D_0 T exp\left(-\frac{E_D}{RT}\right) \tag{5}$$

and

$$P = SD = P_0 T exp\left(-\frac{E_p}{RT}\right) \tag{6}$$

where D_0, S_0 and P_0 ($P_0 = S_0 D_0$) are the coefficients of hydrogen gas diffusion, dissolution and permeation at infinite temperature, respectively and E_D, E_S, E_P ($E_P = E_S + E_D$) are the corresponding activation energies. R is the gas constant (8.314 J K^{-1} mol^{-1}). It should be noted that for gas diffusion in glasses the temperature dependence of the pre-exponential terms in Eqs. (4) and (5) must be taken into account [14].

2.2 Effective hydrogen gas permeation through a glass lined tank

The effective hydrogen gas permeation coefficient *P* through a double layer tank wall (polymer of thickness d_1 with glass lining of thickness d_2) with the intrinsic hydrogen gas permeation coefficients P_1 (polymer) and P_2 (glass lining) was calculated by assuming additivity of the layer thickness $d = d_1 + d_2$ and the associated decrease in the hydrogen partial pressure $p = p_1 + p_2$. For the flux *J* of the diffusing gas with the surface area *A* one has:

$$J = \frac{dQ}{dt}\frac{1}{A} = P\frac{p}{d} \tag{7}$$

The conservation of *J* leads to:

$$P\frac{p}{d} = P_1\ \frac{p_1}{d_1} = P_2\ \frac{p_2}{d_2} \tag{8}$$

The transformation of Eq. (8) leads to the following expression for the total hydrogen partial pressure *p*:

$$p\ = p_1 + p_2 = p\ \left(\frac{P}{P_1}\frac{d_1}{d}\right) + p\ \left(\frac{P}{P_2}\frac{d_2}{d}\right) \tag{9}$$

and

$$p\ = p\ \left[\left(\frac{P}{d}\frac{d_1}{P_1}\right) + \left(\frac{P}{d}\frac{d_2}{P_2}\right)\right] \tag{10}$$

Further rearranging of Eq. (10) gives:

$$\frac{d}{P} = \frac{d_1}{P_1} + \frac{d_2}{P_2} \tag{11}$$

and

$$\frac{P}{d} = \frac{P_1\ P_2}{P_2\ d_1 + P_1\ d_2} \tag{12}$$

Finally, for the effective permeation coefficient of the double-layered wall, we obtain:

$$P = \frac{P_1 P_2}{P_2\left(\frac{d_1}{d}\right)+P_1\left(\frac{d_2}{d}\right)} \tag{13}$$

For d_2 = 0 (no glass lining) and thus $d_1 = d$, the result is e.g. $P = P_1$ (polymer).

3. Results

Fig. 1 shows the decrease in the release rate of hydrogen gas from a cordierite glass powder sample (Mg22.2) at 310 °C, which was used to determine the diffusion coefficient *D* and the final release of remaining hydrogen during heating up to 825 °C. Time integration over the entire duration of the experiment resulted in the total amount of H_2 released (area under the blue line) and was used to determine the solubility *S* of the previous H_2 pressure loading performed at the same temperature. The *D* and *S* values of cordierite and those measured for eucryptite and spodumene glasses were listed in Tab. 1.

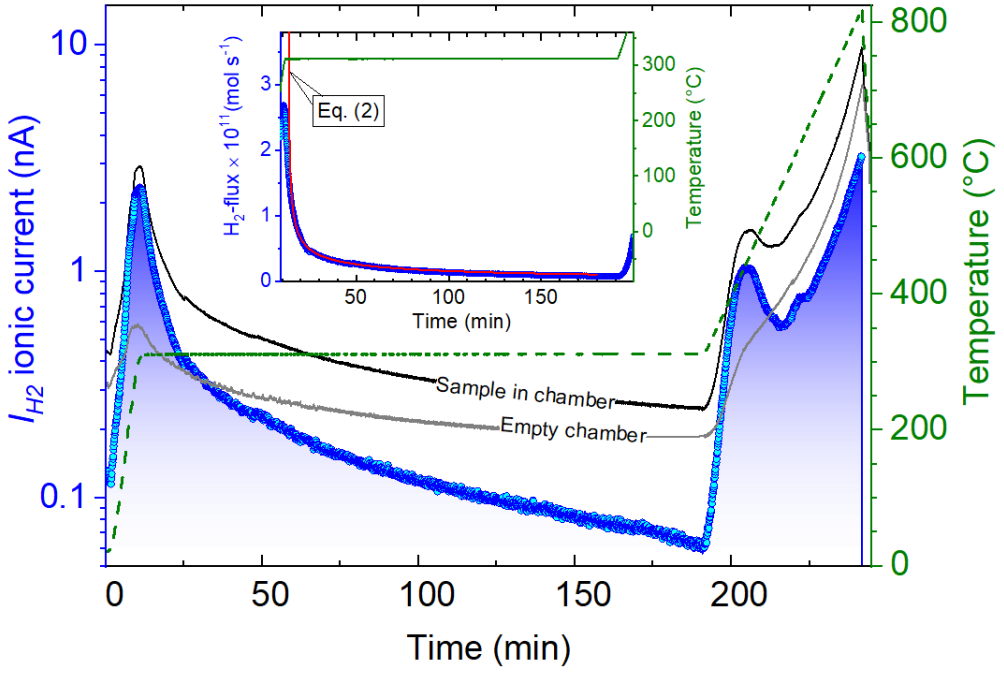

Figure 1. H_2 ionic current (I_{H2}) of a Mg22.2 glass powder sample (blue line) of *m* = 105.3 mg in vacuum after loading at 310 °C and 6 MPa H_2 pressure for 24 h. The integration from 0 to 240 min (blue area under the curve) resulted in the total amount of dissolved H_2 (the calibration constant *C* was 0.011417 mol H_2 A^{-1} s^{-1}). The insert shows the gas release rate *dQ*/*dt* of H_2 (H_2-flux) of the isothermal degassing section and the fit of Eq. (2) on the data (red line) with t_0 = 800 s as the start time of the isothermal degassing step.

Table 1. Hydrogen gas solubility S (mol H_2 m^{-3} Pa^{-1}) and diffusivity D (m^2 s^{-1}) of Li25, Li16.7, and Mg22.2 glasses.

	Li25		Li16.7		Mg22.2	
T (°C)	$10^7 \times S$	$10^{14} \times D$	$10^7 \times S$	$10^{14} \times D$	$10^7 \times S$	$10^{14} \times D$
210	3.06	1.7	16.2	1.55	5.95	0.062
260	2.93	5.1	16.0		3.60	0.16
260	2.49				2.43	
310	1.73	15	11.1		2.68	0.8
310			10.8	18		
310			7.78	28		

Fig. 2 shows Arrhenius plots of the solubility and diffusivity data of Tab. 1. For all three glasses, the hydrogen gas solubility decreases slightly with temperature, while the diffusivity increases more strongly. In comparison, the glass with the spodumene composition (Li16.7) shows the highest solubility and diffusivity values, whereas hydrogen molecules are dissolved least in the eucryptite glass (Li25) and can diffuse least in the cordierite glass (Mg22.2). Fitting Eqs. (4) and (5) to the data resulted in the pre-exponential constants and activation energies listed in Tab. 2.

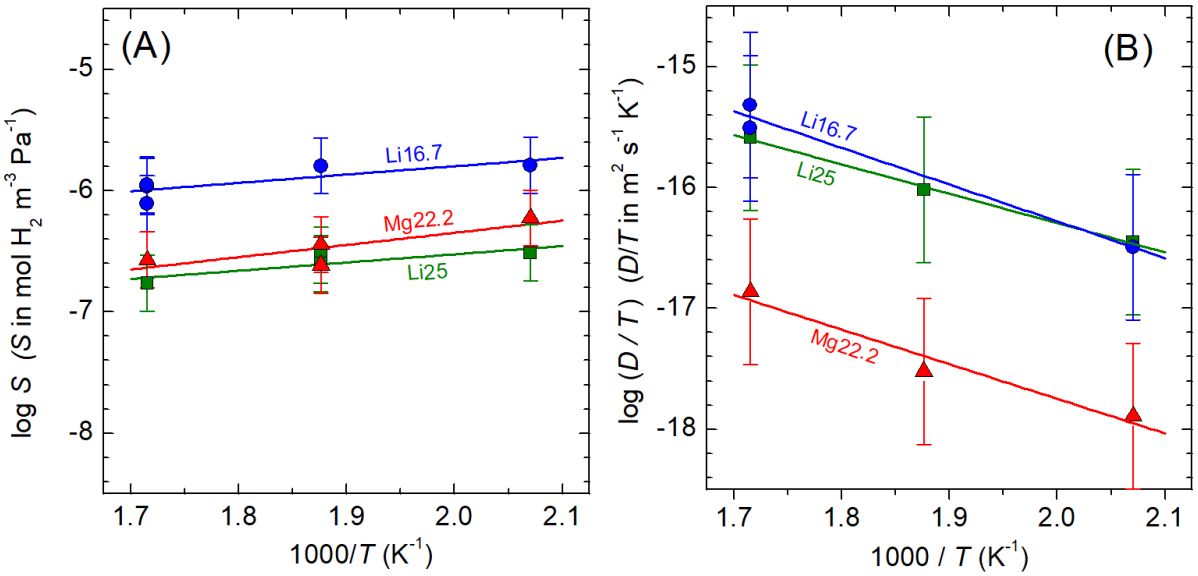

Figure 2. Solubility (A) and diffusivity (B) as a function of temperature of glasses of spodumene (Li16.7), eucryptite (Li25) and cordierite (Mg22.2) composition. Lines are fits of Eqs. (4) and (5) to the data.

Fig. 3 shows the hydrogen gas solubility together with the previously measured diffusivity [8] at 268 °C as a function of Na_2O content of the NAS glasses and the reference silica glass. The dependence on the composition of S and D with increasing SiO_2 content is strongly non-linear with a sharp increase (of solubility) with increasing silica content and a local maximum of S (shoulder for D) at albite composition. The permeability P was calculated from Eq. (6). P was smallest (6.9×10^{-20} mol H_2 (m s Pa)$^{-1}$) for the Na23.8 glass close to the nepheline composition, about three orders of magnitude smaller than the reference silica glass. Since hydrogen solubility was only measured at this temperature, the unknown dependence on temperature, i.e., the parameters S_0 and E_S of NAS glasses, was calculated from the relation between the activation energies for dissolution and diffusion of NBO-free glasses (E_D was taken from [8]). For E_S and E_D in the units kJ mol^{-1} one has [7]:

$$E_S = 2.773 - 0.197 E_D \quad (14)$$

and

$$S_0 = S_{(268°C)} \left[exp\left(-\frac{10^3 E_S}{541\ R} \right) \right]^{-1} \quad (15)$$

Tab. 2 lists all resulting parameters of Eqs. (4)–(6).

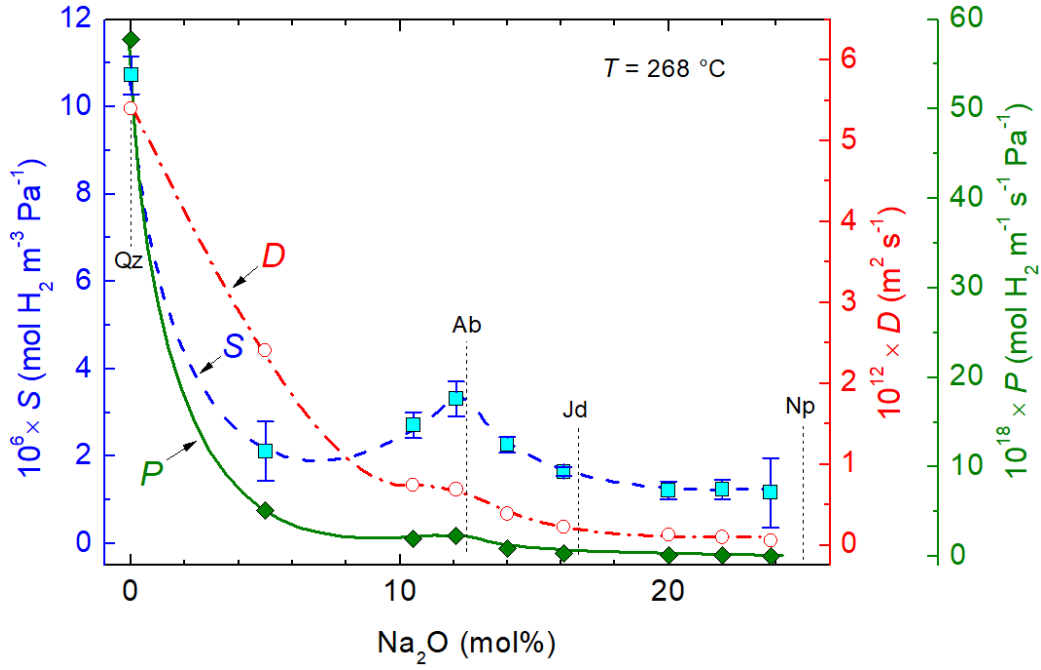

Figure 3. Hydrogen gas solubility *S* (blue left ordinate), diffusivity *D* (red right ordinate) and permeability (green second right ordinate) as a function of the Na_2O content. The *D* data were added from an earlier diffusivity study [8] to highlight the similar composition trend of both parameters. *P* is given by the product *SD*. Compositions for quartz (Qz) and the tectosilicates albite (Ab), jadeite (Jd) and nepheline (Np) are shown. Lines are for visual guidance only.

Table 2. Parameters of Arrhenius Eqs. (4)–(6) of hydrogen gas solubility, diffusivity and permeability, i.e. S_0 (mol H_2 m^{-3} Pa^{-1}), E_S (kJ mol^{-1}), D_0 (m^2 s^{-1} K^{-1}), E_D (kJ mol^{-1}), $P_0 = S_0D_0$ (mol H_2 m^{-1} s^{-1} Pa^{-1} K^{-1}) and $E_P = E_S + E_D$ (kJ mol^{-1}).Specific tectosilicate compositions: spodumene (Spd), eucryptite (Ecp), albite (Ab), jadeite (Jd), nepheline (Np) and reference quartz (Qz). Key: *Data from [8].

System		Glass	Solubility		Diffusivity		Permeability	
			$10^7 \times S_0$	E_S	$10^{12} \times D_0$	E_D	$10^{19} \times P_0$	E_P
LAS	(Spd)	Li16.7	0.677	-13.1	62.8	58.2	42.5	45.1
	(Ecp)	Li25	0.133	-12.9	3.61	46.4	0.48	33.5
NAS		Na5	13.1	-4.9	27.1*	39.2*	191	34.3
		Na10.5	15.6	-5.8	20.8*	43.3*	157.1	37.5
	(Ab)	Na12.1	14.7	-8.4	389*	56.8*	1978.9	48.4
		Na14	12.0	-6.5	26.3*	47.3*	138.8	40.7
	(Jd)	Na16.1	9.46	-5.7	6.09*	43.2*	28	37.5
		Na20	5.33	-8.6	82.5*	57.6*	149.6	49.0
		Na22	5.24	-8.9	94.2*	59.2*	161.6	50.3
	(Np)	Na23.8	4.12	-10.8	474*	68.7*	504.4	58.0
MAS	(Cor)	Mg22.2	0.0438	-19.2	0.952	54.8	0.0417	35.6
S	(Qz)		44.5	-4.0	19.9*	34.2*	883.3	30.2

4. Discussion

To explore the potential of glasses with tectosilicate composition for hydrogen gas barrier linings, the permeability in Fig. 4 was extrapolated to the ambient temperature range and compared with that of conventional polymers. Despite the considerable uncertainty (approximately ±1 log unit) of such a wide extrapolation, it can be seen that linings of these glass compositions can contribute to a significant reduction in hydrogen permeation and thus minimize hydrogen volume losses of after pressurised refuelling over long periods of time. Most striking, the cordierite composition was found to be particularly suitable because its permeation coefficient at 298 K is about 9 orders of magnitude lower than the lowest permeable polymer material (polyamide).

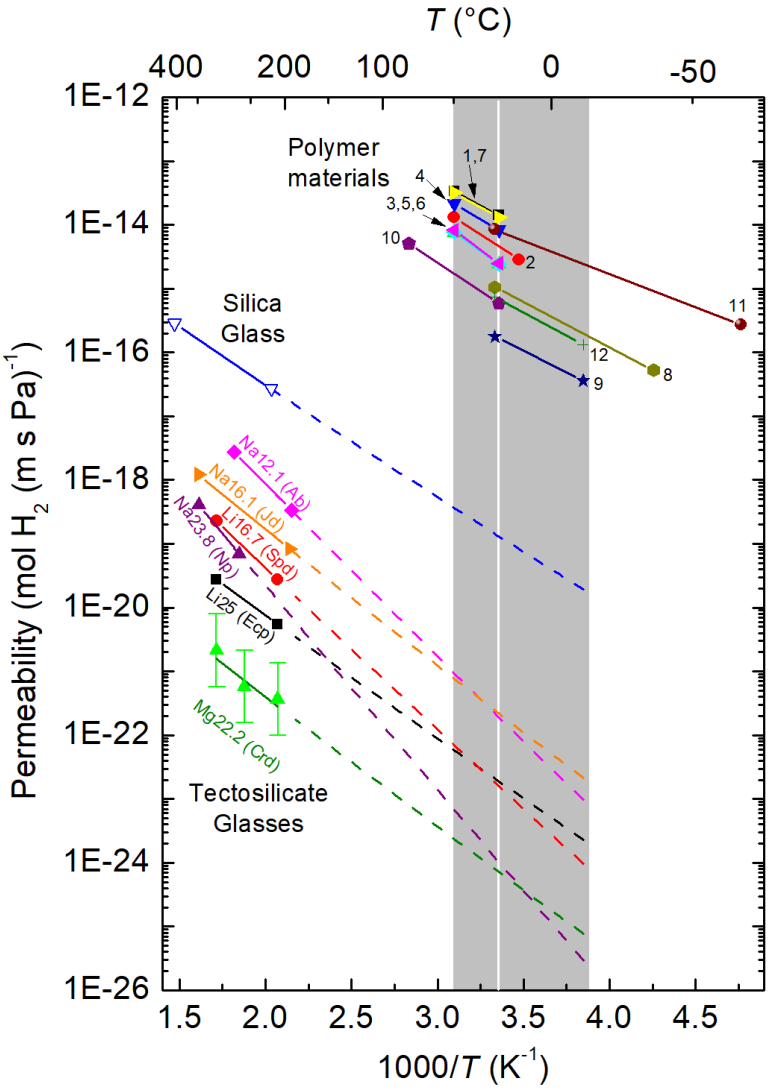

Figure 4. Hydrogen gas permeability of tectosilicate glass compositions in dependence of temperature. Silica reference glass and common polymer materials are shown for comparison. The solid lines indicate measured temperature range while the dashed lines are the extrapolations to the ambient temperature range. For cordierite glass, data points and error bars are added to provide an estimate of the uncertainty of the values in the ambient temperature range. Polymer data were taken from the collection in [5] with 1 = polybutadiene, 2 = neoprene G, 3 = 98/2 isobutene/isoprene, 4 = butadiene/acrylonitrile (perbunan 18 (80/20)), 5 = butadiene/acrylonitrile (Hycar OR 15 (61/39)), 6 = 74/26 isoprene/acrylonitrile, 7 = styrene-butadiene rubber (Buna S), 8 = high-density polyethylen, 9 = polyamide, 10 = polyvinyl chloride, 11 = polyvinyl chloride (unplasticised) and 12 = epoxy LY556/HY917 Ciba Geigy. Standard condition (298 K, white vertical line), ambient temperature range (grey box).

Fig. 5 illustrates the possible reduction in hydrogen permeation that can be achieved with a glass lining. As an example, a spherically capped cylinder (radius r = 0.1 m, cylinder height h = 0.5 m, polymer wall thickness d_1 = 2 cm), a tank pressure of p = 70 MPa, and a glass liner thickness of d_2 =1 µm is considered. The hydrogen permeability of an example polymer (HDPE) and example glass (Li 16.7) at 273 K were taken from Fig. 4 as $P_1 \approx 10^{-15}$ mol H_2 (m s Pa)$^{-1}$ and $P_2 \approx 10^{-23}$ mol H_2 (m s Pa)$^{-1}$, respectively. Simple calculations give a tank volume of V = 0.02 m^3, a surface area of A = 0.44 m^2. Without glass lining (dashed curves), the initial hydrogen loss during the first day

$$\Delta Q = P_1 \, A \frac{p}{d_1} \, 86400 \, s \tag{16}$$

is only 0.268 g (constant pressure during the first day). After 50 days, however, ΔQ reaches 13.3 g H_2, which is already ~149 litres. In this way, dangerous amounts of hydrogen could be accumulated close to the tank environment. On the other hand, hydrogen dissolves into the polymer material at high pressure, which could cause materials degradation phenomena, e.g. promoting formation of microcracks during loading and reloading. With a glass lining, permeation and the hydrogen partial pressure to which the polymer wall is exposed are greatly reduced. Already, a 1 µm thick glass lining of a 2 cm polymer wall would reduce hydrogen leakage by about 4 orders of magnitude to $\Delta Q = 5.4 \times 10^{-5}$ g H_2 after the first day or 2.68×10^{-3} g H_2 after 50 days. Furthermore, according to Eq. (8), the maximum hydrogen partial pressure to which the polymer wall is exposed is about 14×10^3 Pa, i.e. 4 orders of magnitude less than the inner tank pressure.

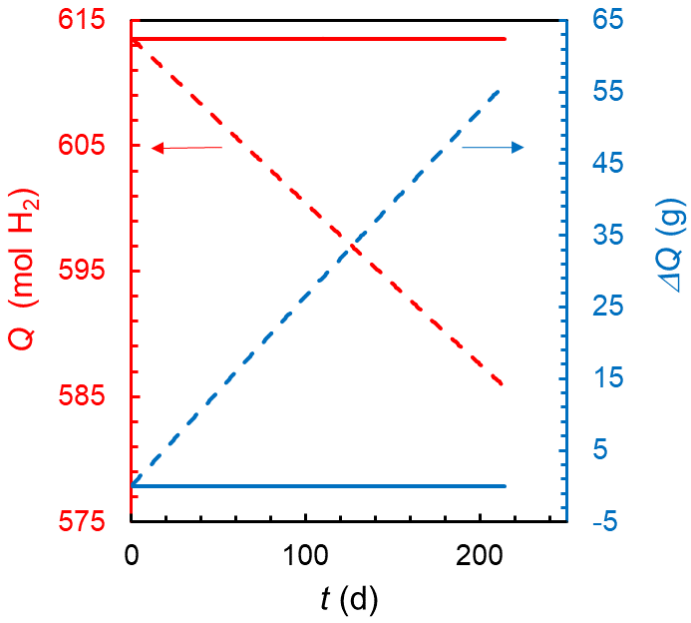

Figure 5. Remaining hydrogen content Q and cumulative hydrogen gas loss ΔQ from a spherically capped polymer cylinder tank (r = 0.1 m, h = 0.5 m) with (solid) and without glass lining (dashed). Polymer wall thickness d_1 = 2 cm, glass liner thickness d_2 = 1 µm.

Fig. 6 shows possible designs of liners on the inside of a carbon-fibre-reinforce polymer (CFRP) composite tank made entirely of glass (left), made from a multilayer thin-glass polymer composite (centre) with very thin overlapping glue joints, and made by a combination of CFRP and glass, i.e. CFRP-sheathed glass capillary bundles (right).

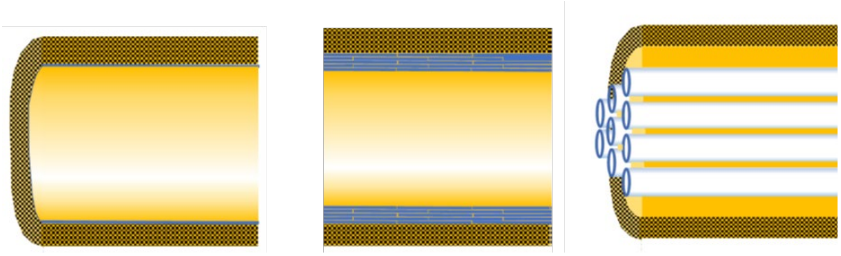

Figure 6. Possible CFRP-glass composite storage concepts. Left: Type IV CFRP storage with glass liner (blue). Middle: Type V CFRP storage with an H_2 diffusion barrier made of thin glass-polymer composite. Right: CFRP-lined glass capillary bundles.

5. Conclusions

Eucryptite, spodumene and cordierite glasses with fully polymerised aluminosilicate network structures showed ultra-low hydrogen gas permeation at 210–310 °C. When extrapolated to room temperature, the permeability was found to be as low as 10^{-22}–10^{-24} mol H_2 (m s Pa)$^{-1}$, 8–10 orders of magnitude lower than that of most polymers. Thin glass linings of this composition are likely to be the most effective barrier for tanks containing compressed hydrogen.

Data availability statement

All original data supporting the results are given in Table 1 and Table 2.

Author contributions

S. Reinsch: Investigation, Methodology, Validation, Writing – review & editing. T. Welter: Investigation, Methodology, Validation, Writing – review & editing. R. Müller: Formal Analysis, Funding acquisition, Project administration, Resources, Supervision, Validation, Visualization, Writing – review & editing. J. Deubener: Conceptualization, Formal Analysis, Funding acquisition, Project administration, Resources, Supervision, Validation, Visualization, Writing – original draft, Writing – review & editing.

Competing interests

The authors declare that they have no competing interests.

Funding

S.R. and R.M. thanks BMWK for the financial support under grant LuFo VI-2 20E2117B. J.D. thanks the Deutsche Forschungsgemeinschaft (DFG) for providing funding under grant DE 598/20-2.

Acknowledgement

The authors thank U. Fotheringham and B. Rüdinger of Schott AG (Mainz, Germany) for glass production.

References

1. B. O. Mysen, “The structure of silicate melts,” Ann. Rev. Earth Planet. Sci., vol. 11, pp. 75–97, 1983, doi: https://www.doi.org/10.1146/annurev.ea.11.050183.000451
2. P. A. Rosen, “Beitrag zur Optimierung von Wasserstoffdruckbehältern, Thermische und Geometrische Optimierung für die automobile Anwendung,“ AutoUni-Schriftenreihe Band 113, Springer, Wiesbaden, 2018, pp. 11–130.
3. Y. Su, H. Lv, W. Zhou and C. Zhang, “Review of the hydrogen permeability of the liner material of type iv on-board hydrogen storage tank,” World Electr. Veh. J., vol. 12, Art. no. 130, 2021, doi: https://www.doi.org/10.3390/wevj12030130
4. M. Prewitz, M. Gaber, R. Müller, C. Marotztke and K. Holtappels, “Polymer coated glass capillaries and structures for high-pressure hydrogen storage: permeability and hydrogen tightness,” Int. J. Hydro. Energ., vol. 43, pp. 5637–5644, 2018, doi: https://www.doi.org/10.1016/j.ijhydene.2017.12.092
5. R. R. Barth, K. L. Simmons and C. San Marchi, “Polymers for hydrogen infrastructure and vehicle fuel systems: applications, properties, and gap analysis,” Sandia National Labs., Albuquerque, NM, USA, Livermore, CA, USA, 2013, p. 34.
6. J. E. Shelby, “Handbook of diffusion in solids and melts,” ASM International, Chicago 1996, pp. 16–70.
7. T. Welter, R. Müller, J. Deubener, U. Marzok and S. Reinsch, “Hydrogen permeation through glass,“ Front. Mater., vol. 6, Art. no. 342, 2020, doi: https://www.doi.org/10.3389/fmats.2019.00342
8. T. Welter, U. Marzok, J. Deubener, S. Reinsch and R. Müller, “Hydrogen diffusivity in sodium aluminosilicate glasses,“ J. Non-Cryst. Solids, vol. 521, Art. no. 119502, 2019, doi: https://www.doi.org/10.1016/j.jnoncrysol.2019.119502
9. A. Zandona, B. Rüdinger, O. Hochrein and J. Deubener, “Crystallization sequence within the keatite solid solution – cordierite mixed compositional triangle with TiO_2 as nucleating agent,” J. Non-Cryst. Solids vol. 505, pp. 320–332, 2019, doi: https://doi.org/10.1016/j.jnoncrysol.2018.11.012
10. R. M. Barrer, “Diffusion in and through solids,” Cambridge Univ. Press, Cambridge, 1941, pp. 117–143.
11. P. Ried, M. Gaber, R. Müller and J. Deubener, “Hydrogen permeability of a barium-aluminoborosilicate glass - A methodical approach,” J. Non-Cryst Solids, vol. 394-395, pp. 43–49, 2014, doi: https://www.doi.org/10.1016/j.jnoncrysol.2014.04.006
12. J. Crank, “The Mathematics of Diffusion,” 2nd ed., Oxford Univ. Press, Oxford, 1975, pp. 89–103.
13. R. H. Doremus, “Glass Science,” 2nd ed., John Wiley & Sons, New York, 1994, pp. 122–150.
14. J. E. Shelby and S. C. Keeton, “Temperature dependence of gas diffusion in glass,” J. Appl. Phys., vol. 45, pp. 1458–1460, 1974, doi: https://www.doi.org/10.1063/1.1663433